Digital-image-correlation observation of cyclic plastic strain field during the damage-accumulation mode of fatigue crack propagation under pure cyclic mode II loading for cold-rolled SUS430 steel

Hamada, Shigeru
Faculty of Engineering, Kyushu University

Araki, Yamato
Graduate School of Engineering, Kyushu University

Noguchi, Hiroshi
Faculty of Engineering, Kyushu University

出版情報：Materials Science and Engineering : A. 845, pp.143246-, 2022-06-15. Elsevier
バージョン：
権利関係：

Digital-image-correlation Observation of Cyclic Plastic Strain Field during the Damage-accumulation Mode of Fatigue Crack Propagation under Pure Cyclic Mode II Loading for Cold-rolled SUS430 Steel

Shigeru Hamada [a*], Yamato Araki [b], and Hiroshi Noguchi [a]

[a] Faculty of Engineering, Kyushu University, 744 Moto-oka, Nishi-ku, Fukuoka-shi, Fukuoka 819-0395, Japan

[b] Graduate School of Engineering, Kyushu University, 744 Moto-oka, Nishi-ku, Fukuoka-shi, Fukuoka 819-0395, Japan

[*]Corresponding author: hamada@mech.kyushu-u.ac.jp

Abstract

Fatigue cracks propagate intermittently by the cyclic initiation and coalescence of voids in front of the fatigue crack tip during fatigue crack propagation in the damage accumulation mode. In this study, digital image correlation is used to measure the evolution of the measured plastic strain distribution near the crack tip with loading and cyclic loading during one cycle. The evolution is estimated based on strain distribution measurements results and mechanical considerations. The strain is set at the unloading point because results indicate that the crack propagated in the region where the experimental shear plastic strain is the maximum in the first quarter cycle (at the first maximum load); the measured plastic strain is almost constant in the region where the crack propagates, and the crack is initiated by a subsequent cyclic strain localization and coalescence with the main crack. This study clarified the damage accumulation mode fatigue crack propagation mechanism with the measured strain behavior, and presents a method to use continuum plastic strain at the crack tip as a mechanical driving force for this mode.

Keywords: Fatigue crack propagation, Damage accumulation mode, Cyclic Mode II loading, Plastic strain, Strain concentration, Cyclic strain localization

1. Introduction

Fatigue cracks often extend on the plane where principal stress acts [1-3] in the tensile mode [1] when a metallic material with a crack is subjected to cyclic Mode II [4-6] loading. However, in some materials, the crack propagates on the plane under certain conditions where the maximum shear stress acts [1, 7-12] in the shear mode [1]. Shear mode fatigue crack propagation (FCP) can occur in the same material and under the same conditions; however, its behavior is highly variable when it occurs [13]. Therefore, shear mode fatigue crack extension is speculated to be different from that in the tensile mode, not only in its fatigue crack extension path and mechanical driving force but also in terms of its fatigue crack extension mechanism.

In this study, the authors introduced a sharp notch (pre-crack) into cold-rolled ferritic stainless steel SUS430, which had texture, and they applied cyclic Mode II loading. The results indicated that the process of void initiation, growth, and coalescence in front of the crack proceeded with a cyclic external force; the voids became secondary fatigue cracks and the crack coalesced with the main crack, which was the mechanism of discontinuous crack propagation [13-15]. Further, the tensile mode fatigue crack extension was named plastic deformation (PD) mode fatigue crack growth (FCG) based on the fatigue crack extension mechanism, and the shear mode fatigue crack extension was named damage accumulation (DA) mode FCP [13]. They were classified to extend the study of shear mode FCP from passive to FCP simulation by coarse-graining the material based on the FCP mechanism, as in the case of plasticity-induced crack closure simulation with residual PD in the wake of the fatigue crack tip in the PD-mode FCG [16-20]. In addition, the conventionally used names such as Mode II FCP [21], Mode II FCG [22], and shear mode FCG [23] are all based on the loading mode; these names are not based on the FCP mechanisms.

In fatigue crack initiation, voids are initiated by the accumulation of positive and negative dislocations, formation of vacancies, and accumulation of vacancies [24-28]. In the DA-mode FCP, secondary fatigue cracks are initiated sequentially in front of the fatigue crack tip by void coalescence. Further, the nominal

cyclic shear plastic strain range $\Delta\gamma^p$ has been empirically used as a mechanical driving force for controlling the fatigue crack initiation life of smooth specimens [29-32]. A high local plastic strain dominates the phenomenon because fatigue crack initiation is a localized phenomenon. This can be explained by considering that the nominal plastic strain dominates the localization of the local plastic strain. McDowell-Dunne [33] introduced “fatigue indicator parameters” for fatigue crack formation in polycrystalline microstructures and the concept of microplasticity within individual grains as a critical driving force parameter. Castelluccio-McDowell [34] discussed averaging the driving force and concluded that grain-based averaging is optimal. One question for materials with a crack is how to define the nominal cyclic plastic strain in the case of strain concentration by the crack.

A mechanical driving force used to predict the DA-mode FCP can be a crack-induced, concentrated [35] continuum plastic strain because the continuum plastic strain can be analyzed mechanically and is reproducible. In conventional fracture mechanics, the intensity of a singular field at the crack tip is used. However, the above-mentioned problem cannot be solved by simply assuming that the DA-mode FCP occurs in this singular field. Further, it is possible that the change in the plastic strain range can be obtaining the crystal information of the individual crystals near the crack tip and performing crystal plasticity finite element method iterations [32, 33]. If the mechanical designer has access to all the crystal information near the crack tip in the actual machine, the DA-mode FCP can be predicted from the microstructure. However, this method cannot be currently employed in actual machines. Although the concept of the nominal cyclic strain is extended in this study, continuum plastic strain is used in this study. To this end, it is necessary to understand the relationship between the continuum strain distribution near the crack tip and actual strain. The continuum plastic strain near the crack tip was distributed and varied with the loading cycle. The following two issues necessary for the FCP simulation were solved. To predict rationally, (1) in which region and at what timing in cyclic loading should the continuum plastic strain be used? (2) How can the microstructure near the crack tip be quantitatively evaluated? In this study, the authors focus on (1); (2) will be solved in the following paper.

It is preferrable to use a simple material for this study because it makes it easier to understand the

phenomena. To this end, cold-rolled SUS430 steel used in a previous study [13-15] was utilized; SUS430 is a single-phase ferritic stainless steel that contains Cr, and neither Ni or Mo undergoes strain-induced transformation. The cold-rolling process produces texture prone to the DA-mode FCP. Therefore, the fatigue test method developed by the authors [13-15], which allows pure cyclic Mode II loading while observing crack propagation behavior, was adopted. Owing to the limitation of the test method, the strains can be observed only in the unloaded condition. The plastic strain distribution in the loaded condition was estimated from the observed results in the unloaded condition because the plastic strain range is necessary for predicting the propagation behavior of fatigue cracks. Plastic strain observed by the digital image correlation (DIC) method [36] was used as an observable engineering experimental strain (hereafter referred to as the real plastic strain). Strain distribution analysis near the crack tip using the DIC method was performed by Carroll et al. [37]. However, the resolution of the DIC method was several tens of microns, and this is insufficient for this study. The low resolution is attributed to the Vickers indentation used as the speckle pattern, which is a random pattern necessary for the DIC method. Tasan et al. [38] performed a DIC method using the crystal microstructure revealed by etching as a speckle pattern; however, the resolution was similar. In this study, the size of the plastic zone in the crack extension direction was expected to be several tens of microns. Therefore, a more acceptable resolution was required. In this study, the authors applied the μ-DIC method [39-42] developed by Tasan et al. using colloidal silica as a speckle pattern to observe the strain distribution in a narrow region near the crack tip. A spatial resolution of less than micrometers can be expected because the particle size of the colloidal silica is approximately 50 nm.

Furthermore, DIC measurement conditions were optimized to correspond with the continuum plastic strain distribution. The target measurement condition was the reference length in the engineering strain. The micrometer-order deformation of the real material is affected by the microstructure and differs from the deformation of a continuum body because the real plastic strain is for a real material; the setting of the reference length strongly influences the measured plastic strain. Issue (1) is solved through the measurement and analysis of the observable real plastic strain behavior.

2. Experiment method

2.1 Material

For the test, the authors used commercially available cold-rolled thin sheets of ferritic stainless steel SUS430 with uniform thickness, which is the same material used in a previous study [13-15]. Table 1 lists the chemical composition of SUS430. Tensile test specimens were cut from this plate to measure the rolling direction (RD) and transverse direction (TD) properties. The dimensions of the parallel section of the specimen were 25 × 6 × 0.03 mm. The Young's modulus, 0.2% proof stress, and ultimate tensile strength obtained from these specimens were 209 GPa, 1089 MPa, and 1078 MPa for the RD and 238 GPa, 1168 MPa, and 1226 MPa for the TD, respectively. The specimen in the RD direction failed before it reached a sufficient strain to obtain a 0.2% proof stress. Therefore, the 0.2% proof stress is an estimated value obtained by extrapolating the stress–strain relationship.

2.2 Fatigue test

The test method was the same as that proposed by the authors [13-15]. Figure 1 shows a schematic of the test specimen [13]. The specimen was a thin film disc with a 3 mm diameter and 30 μm thickness and it had a 400 μm long notch made with a focused ion beam (FIB) [43] introduced in the center. The longitudinal direction of the notch was set to be the same as that of the RD, where the fatigue crack is known to propagate. The stress ratio was $R = -1$, and the shear stress applied to the test jig was $\tau = \pm 200$ MPa. The test jig was detached from the test machine after a specified number of cycles, and the material behavior near the crack tip was observed using scanning electron microscopy (SEM). A JEOL JSM IT-500 instrument was used as the SEM system.

2.3 DIC analysis

The plastic strain around the crack tip was observed using DIC analysis based on the SEM images, and the change in the plastic strain as a function of the number of loading cycles was investigated. The software used was VID-2D by Correlated Solutions, Inc. The DIC analysis was used, and because the surface of SUS430 was not applicable to the DIC analysis by etching, a random pattern was added to the

surface using colloidal silica to create a speckle pattern required for the DIC analysis. All DIC analyses were based on pre-test images shown in Fig. 2; i.e., the number of loading cycles was $N = 0$.

2.4 Cyclic Mode II loading

The loaded shear stress in the fatigue test had a sinusoidal waveform. The cycles are defined as follows: 0.25 cycle represent positive shear stress loading; 0.5 cycles, unloading; 0.75 cycles, negative shear stress loading; and one cycle, unloading. The plastic strain was observed not only after one cycle of loading, but also after 0.5 cycles of loading to observe how the difference between positive and negative shear stress loading affects the plastic strain distribution.

2.5 Observation method

In the fatigue tests, the brightness, contrast, and focus of the image taken after the test and the reference image at 0 cycles were adjusted to be the same to enable analysis using the DIC method with a high degree of accuracy when the SEM was used to capture the image near the crack. The conventional tests using the DIC method was performed using SEM [39-42]. However, in the present study, the test jig was detached from the testing machine after a specified number of cycles, and near the fatigue crack tip was observed using SEM. In the SEM observation, the inclination of the test jig affected the accuracy of the DIC analysis. The flat surface of the gripping part of the test jig, which was used to attach the test jig to the testing machine is shown in Fig. 1, and it was always horizontal during the SEM observation. In other words, a jig was used to fix the circumferential rotation of the test jig using a level, and the flat surface of the gripping part of the test jig was fixed horizontally when performing the SEM observation. In the absence of this jig, the test jig rotated in the axial or circumferential direction, which changed the observation area; as a result, a pseudo strain was observed throughout the observation area in the DIC analysis.

The strain distribution in the region below the microstructure size was the target of the measurement. Using the DIC method, the deformation from which strain values are calculated is affected by the microstructure. Therefore, the reference length (length before deformation) set by the DIC method for

strain measurement affects the measurement results. Thus, a study was conducted to obtain an appropriate reference length for the measurement results.

After the fatigue test, microstructural analysis using the electron backscatter diffraction (EBSD) method was conducted to observe the state of the texture. The equipment used for the analysis was the Hitachi High-Technologies SU6600. Inverse pole figure (IPF) maps of thin film specimens in the RD, TD, and normal direction were obtained. The FCP plane was the TD plane because the FIB notch was introduced parallel to the RD.

3. Results

3.1 Fatigue crack propagation

Figure 3 shows the FCP behavior as a function of the number of cycles, and the tip of the FIB notch shows that the fatigue crack propagates as a function of the number of cycles. Therefore, the fatigue crack propagated from the tip of the FIB notch according to the number of cycles. Further, the crack propagates along the path where the shear stress is the maximum, which indicates the DA-mode FCP.

3.2 Evolution in shear plastic strain distribution according to the number of cycles *N*

Figure 4 shows the evolution of the shear plastic strain distribution for each number of cycles. In Fig. 4(b), at $N = 0.5$, i.e., after positive shear stress loading and unloading, a region of negative shear strain and a region of positive shear strain is observed in front of the FIB notch. In Fig. 4(c), positive and negative shear stresses were applied after $N = 1$ cycles, i.e., the distribution of shear plastic strain was approximately the same as $N = 0.5$, however, there was a slight change in the positive shear plastic strain region. Fig. 4(d) shows that at $N = 5$ cycles, the shear plastic strain region spread in the crack growth direction compared to the $N = 1$ cycles. In the direction perpendicular to crack propagation, the shear plastic strain region was extended to a lesser extent than the extension in the crack propagation direction.

3.3 Relationship between fatigue crack and shear plastic strain zone

Figure 5 shows the location of fatigue cracks initiated from the FIB notch superimposed on the shear

plastic strain distribution. At all times, the fatigue crack propagates in the region between the positive and negative strains, wherein the residual strain is low. As shown in Fig. 5, the residual strain is present in the wake of the FCP.

3.4 Relationship between shear plastic strain zone and "unit"

Figure 6 shows the IPF map obtained by the EBSD observation after the fatigue test (N = 20 cycles). The authors proposed that dislocations accumulate because of cyclic shear loading in a region called "unit" [13-15], which has the same crystallographic orientation that results in the DA-mode FCP [13]. Although the crystal orientation is disordered because the observation is made after the fatigue test, Figure 6 shows that there are "units" in which the (110) plane, which is a slip plane, is aligned, and the fatigue crack propagates in the "unit." In addition, the region of high shear plastic strain coincides with the region of the "unit."

4. Discussion

4.1 Appropriate reference length for the strain measurement by DIC method

Unlike strain in a continuum body, the strain in a real material with crystals has crystal-dependent nonuniformity [44]. Therefore, it is necessary to compare the strains before and after deformation when measuring the strain. However, the measured strain is affected by the length before deformation owing to this nonuniformity. The reference length should be set carefully when measuring the strain using DIC. Figure 7 shows the distribution of shear strains obtained by setting an inappropriate reference length. The test conditions in Fig. 7 are the same as those in Fig. 4, but for a different specimen. Figure 7 clearly shows an inappropriate strain distribution. The results used in this study were obtained by considering an appropriate reference length.

4.2 Real shear strain estimation caused by cyclic pure Mode II loading

Shear strains obtained by the DIC method do not occur in the entire area of the same crystallographic orientation, which is referred to as a unit, but in a part of the unit. This phenomenon indicates that the shear

strain is not uniformly distributed throughout the unit but is localized because of the slip of single or multiple nearby slip planes within the unit.

Figure 8 shows a schematic of the evolution of the high-strain region with cyclic loading. As an example of a high-strain region, the shear strain values were set to more than 2%. The figure shows residual shear strain during the unloading. As shown in Fig. 8(a), tracing DIC measurement results and the shape of the FIB notch shows that, for the $N = 0.5$ cycle, i.e., the first positive loading, a region of positive shear strain is generated from the crack tip. This region changed its position with the loading cycle, and the crack propagated between the positive and negative high-strain regions. In Fig. 8, the residual shear strain at the unloading is small where the crack propagates, except during the initial period, which suggests that the region is subjected to alternating positive and negative shear strains during cyclic loading. This alternating effect reduced the residual shear strain during unloading.

As shown in the results and focusing on the shear strain caused by loading, each unit is composed of several regions, and some of the regions have a high shear strain, and some have low shear strain. In the following discussion, the authors refer to the regions of a unit as cells to simplify the complex phenomenon. Thus, the behavior of a material subjected to cyclic loading is discussed by considering the material composed of units and their constituent cells.

The measured shear plastic strain in the unloaded state is not sufficient to discuss the material behavior of each cell; the shear plastic strain in the loaded state during one cycle (positive loading-unloading-negative loading-unloading) is also required. Therefore, the shear plastic strain in each cell at $N = 0.25$ and 0.75 cycles, i.e., under loading conditions, is predicted based on the measurement results at $N = 0.50$ and 1.0 cycles. The targets were cells where fatigue cracks propagated (Cell 1, shown in Fig. 9) and the cells where positive and negative shear plastic strains occurred (Cells 2 and 3).

The prediction was performed in three steps, as described below. Results obtained from measurements indicate that the localized slip occurred near the crack tip. Therefore, (1) the authors first predicted the shear stress under the assumption of a continuum body. In this procedure, a deformation easy to visualize is first predicted instead of directly predicting the shear plastic strain, and based on this deformation, the shear

stress corresponding to the deformation is predicted. (2) The next step is predicting the shear stress considering the localized slip that has occurred. (3) Finally, the shear plastic strain is predicted using the stress–strain relationship.

As described above, this study did not directly deal with stress and strain, which are difficult to image; however, it predicted deformations, which are easy to image and thus less likely to cause errors. This method represents the originality of this study. Figure 9 shows the results of the final prediction of shear plastic strain.

Figure 10 shows the predicted shear stress assuming a continuum body. As shown in the figure, the correspondence between the gradient of deformation and the shear stress and the areas of positive and negative shear stress are equal when unloading. Figure 11 shows the predicted shear stress based on Fig. 10 considering the slip in each cell and other regions where local shear strain occurs. Finally, Fig. 12 shows the evolution of the relative shear plastic strain as a function of the number of cycles for each cell, which summarizes the above results.

The experiment results yield the evolution of the shear plastic strain in each cell near the crack tip. Based on the results, the behavior of shear plastic strain, which is the basis for the non-reproducible phenomenon of fatigue crack extension, is divided into non-reproducible and reproducible sections. For the division, the authors introduce the following assumptions: First, the fatigue test results show that the generated shear plastic strain is already high in the first 0.5 cycles. Subsequently, the magnitude of the shear plastic strain is increased with the number of cycles in the same region. Therefore, the cause of the variation in the FCP behavior may be attributed to the distribution of plastic shear strain that occurs up to the first 0.5 cycle.

4.3 Damage accumulation mode fatigue crack propagation mechanism described by real shear plastic strain

Shear plastic strain distribution obtained from the present experiments is considerably different from the strain distribution obtained by continuum mechanics under static loading [5]. Further, the effects of

cracks and crystal microstructures are different in monotonic and cyclic loading processes.

The DA-mode FCP mechanism is determined using the estimated plastic strain behavior as follows: The DA-mode fatigue cracks propagated in the region where the real shear plastic strain was the maximum during a quarter cycle (at the first maximum loading). During the quarter cycle, real plastic strain is almost constant in the unit cell, i.e., in the FCP unit. Thus, fatigue cracks are initiated, coalesced, and propagated because of the strain localization caused by cyclic loading in the unit cell.

4.4 Evaluation strategy for damage accumulation mode fatigue crack propagation

In the previous section, an FCP mechanism was described using real strain behavior. Therefore, the mechanical driving force of FCP in the DA-mode can solve issues discussed in the introduction. Figure 13 shows a specific evaluation policy, wherein the evaluation method is constructed along the black line, and the prediction is carried out along the red dashed line.

The behavior of each element is expressed as continuum body behavior and real material behavior. The behavior of a real material can be observed visually; however, it cannot be predicted using only the visually observed results. The causes required to solve this issue remain invisible; further, the authors introduce meso-behavior between macro-behavior and micro-behavior for the generalization. Macroscopic behavior varies greatly with individual conditions, whereas microscopic behavior is generalizable but too far away for individual boundary conditions in the issue. Thus, for generalization, it is necessary to consider the intermediate behavior of the meso-behavior.

The cause of the FCP is assumed to be the average continuum strain based on the strength mechanism of the real material behavior. The strength characteristics of real materials are described by the relationship between the number of crack initiation cycles N_i and the average continuum strain $\Delta\varepsilon^p$ ($\Delta\gamma^p$). The average continuum strain was derived from the external force of the actual material to predict the FCP. It is necessary to consider the microstructure of the actual machine because the DA-mode FCP is greatly affected by the microstructure. However, the observed microstructure cannot be directly considered for the material at the crack tip, which is related to crack propagation, because the microstructure of an actual

machine is complex. Thus, it is necessary to extract only the essence of the material to be considered. In other words, coarse graining was necessary. The lifetime of an actual machine can be predicted by combining the strength properties and coarse-grained material properties with the average continuum strain, which is the mechanical driving force.

The demonstration of the strategy described above for evaluating the DA-mode FCP will be presented in the authors' future study.

5. Conclusions

The DA-mode FCP is based on the initiation and coalescence of voids attributed to cyclic loading. It is necessary to establish the mechanical driving force for the FCP to predict the fatigue life. In this study, the μ-DIC method was used to observe the evolution of the real plastic strain distribution near the crack tip depending on the number of loading cycles to understand the real strain behavior corresponding to the void behavior under cyclic loading. The strain can only be measured during unloading because of the limitation of the test method, and therefore, the evolution of strain distribution under cyclic loading was estimated based on the measured strain distribution during the unloading and mechanical discussion. Thus, the following FCP mechanisms described using real strain behavior are clarified.

1) DA-mode fatigue cracks are propagated through the maximum real shear plastic strain region in the first quarter cycle (at the first maximum loading).
2) During a quarter cycle, the real plastic strain is almost constant in the cell, which is the unit of propagation.
3) Fatigue cracks are initiated, coalesced, and propagated because of strain localization caused by cyclic loading in the cell.

As described above, the FCP mechanism can be described using the real strain behavior, which provides opportunities to use the continuum plastic strain near the crack tip as the mechanical driving force for DA-mode FCP.

Acknowledgments

This work was financially supported by JSPS KAKENHI (JP16H06365). We would like to thank Editage (www.editage.com) for English language editing.

References

[1] A. Otsuka, K. Mori, T. Miyata, The condition of fatigue crack growth in mixed mode condition, Engineering Fracture Mechanics 7(3) (1975) 429-432,IN15-IN18,433-439, https://doi.org/10.1016/0013-7944(75)90043-0.

[2] P.E. Bold, M.W. Brown, R.J. Allen, A review of fatigue crack growth in steels under mixed Mode I and II loading, Fatigue & Fracture of Engineering Materials & Structures 15(10) (1992) 965-977, https://doi.org/10.1111/j.1460-2695.1992.tb00025.x.

[3] V. Doquet, G. Bertolino, Local approach to fatigue cracks bifurcation, International Journal of Fatigue 30(5) (2008) 942-950, https://doi.org/10.1016/j.ijfatigue.2007.06.001.

[4] G.R. Irwin, Fracture, in: S. Flügge (Ed.), Encyclopedia of Physics Volume VI: Elasticity and Plasticity, Springer, Berlin, 1958, pp. 551-590.

[5] F.A. McClintock, G.R. Irwin, Plasticity aspects of fracture mechanics, in: J. W. F. Brown (Ed.), ASTM Special Technical Publication 381 (STP 381): Fracture Toughness Testing and Its Applications, American Society for Testing and Materials, Philadelphia, PA, 1965, pp. 84-113, https://doi.org/10.1520/STP26586S.

[6] J.R. Rice, Mathematical analysis in the mechanics of fracture, in: H. Liebowitz (Ed.), Fracture: An Advanced Treatise (Vol. 2, Mathematical fundamentals), Academic Press, New York, 1968, pp. 191-311.

[7] P.E. Bold, M.W. Brown, R.J. Allen, Shear mode crack growth and rolling contact fatigue, Wear 144(1–2) (1991) 307-317, https://doi.org/10.1016/0043-1648(91)90022-m.

[8] Y. Murakami, S. Hamada, A new method for the measurement of Mode II fatigue threshold stress intensity factor range $\Delta K_{\tau th}$, Fatigue & Fracture of Engineering Materials & Structures 20(6) (1997) 863-870, https://doi.org/10.1111/j.1460-2695.1997.tb01530.x.

[9] V. Doquet, Q.H. Bui, G. Bertolino, E. Merhy, L. Alves, 3D shear-mode fatigue crack growth in maraging steel and Ti-6Al-4V, International Journal of Fracture 165(1) (2010) 61-76, https://doi.org/10.1007/s10704-010-9504-7.

[10] H. Matsunaga, M. Makizaki, D.F. Socie, K. Yanase, M. Endo, Acceleration of fatigue crack growth due to occasional mode II loading in 7075 aluminum alloy, Engineering Fracture Mechanics 123(0) (2014) 126-136, https://doi.org/http://dx.doi.org/10.1016/j.engfracmech.2014.04.015.

[11] M. Endo, S. Okazaki, H. Matsunaga, S. Moriyama, K. Munaoka, K. Yanase, A New Fatigue Testing Machine for Investigating the Behavior of Small Shear-Mode Fatigue Cracks, Experimental Techniques 40(3) (2016) 1065-1073, https://doi.org/10.1007/s40799-016-0102-0.

[12] S. Hamada, K. Zhang, J. Zhang, M. Koyama, T. Yokoi, H. Noguchi, Effect of shear-affected zone on

fatigue crack propagation mode, International Journal of Fatigue 116 (2018) 36-47, https://doi.org/10.1016/j.ijfatigue.2018.06.003.

[13] S. Hamada, K. Zhang, M. Koyama, M. Ueda, H. Noguchi, Fatigue crack propagation modes: Plastic deformation mode and damage accumulation mode, International Journal of Fracture 222(1) (2020) 111–122, https://doi.org/10.1007/s10704-020-00433-7.

[14] S. Hamada, T. Suemasu, S. Fukudome, M. Koyama, M. Ueda, H. Noguchi, Roughness-induced stress shielding effect in fatigue crack propagation under Mode II loading, International Journal of Fatigue 116 (2018) 245-256, https://doi.org/10.1016/j.ijfatigue.2018.06.029.

[15] S. Hamada, T. Suemasu, M. Koyama, M. Ueda, H. Noguchi, Re-examination of fatigue crack propagation mechanism under cyclic Mode II loading, Procedia Structural Integrity (Proceedings of 22nd European Conference on Fracture (ECF22), Belgrade, Serbia) 13 (2018) 1026-1031, https://doi.org/10.1016/j.prostr.2018.12.191.

[16] B. Budiansky, J.W. Hutchinson, Analysis of closure in fatigue crack growth, Transactions of the ASME, Journal of Applied Mechanics 45(2) (1978) 267-276, https://doi.org/10.1115/1.3424286.

[17] J.C. Newman Jr, Crack-closure model for predicting fatigue crack growth under aircraft spectrum loading, in: J.B. Chang, C.M. Hudson (Eds.), ASTM Special Technical Publication 748 (STP 748): Methods and Models for Predicting Fatigue Crack Growth under Random Loading, American Society for Testing and Materials1981, pp. 53-84.

[18] K. Tanaka, Y. Akiniwa, Y. Nakai, R.P. Wei, Modelling of small fatigue crack growth interacting with grain boundary, Engineering Fracture Mechanics 24(6) (1986) 803-819, https://doi.org/10.1016/0013-7944(86)90266-3.

[19] N. Fukumura, T. Suzuki, S. Hamada, K. Tsuzaki, H. Noguchi, Mechanical examination of crack length dependency and material dependency on threshold stress intensity factor range with Dugdale model, Engineering Fracture Mechanics 135 (2015) 168-186, https://doi.org/10.1016/j.engfracmech.2015.01.003.

[20] N. Fukumura, B. Li, M. Koyama, T. Suzuki, S. Hamada, K. Tsuzaki, H. Noguchi, Material property controlling non-propagating fatigue crack length of mechanically and physically short-crack based on Dugdale-model analysis, Theoretical and Applied Fracture Mechanics 90 (2017) 193-202, https://doi.org/10.1016/j.tafmec.2017.04.012.

[21] R. Roberts, J.J. Kibler, Mode II fatigue crack propagation, Transactions of ASME, Journal of Basic Engineering 93(4) (1971) 671-680, https://doi.org/10.1115/1.3425325.

[22] J. Tong, J.R. Yates, M.W. Brown, A model for sliding mode crack closure. Part I. Theory for pure Mode II loading, Engineering Fracture Mechanics 52(4) (1995) 599-611, https://doi.org/10.1016/0013-7944(95)00044-V.

[23] M. Klesnil, P. Lukáš, Dislocation structure associated with fracture surface of fatigued copper single crystals, Philosophical Magazine 17(150) (1968) 1295-1298, https://doi.org/10.1080/14786436808223204.

[24] T.-G. Zhai, S. Lin, J.-M. Xiao, Influence of non-geometric effect of PSB on crack initiation in aluminium single crystal, Acta Metallurgica et Materialia 38(9) (1990) 1687-1692,

https://doi.org/10.1016/0956-7151(90)90011-5.

[25] T. Zhai, J.W. Martin, G.A.D. Briggs, Fatigue damage in aluminum single crystals—I. On the surface containing the slip burgers vector, Acta Metallurgica et Materialia 43(10) (1995) 3813-3825, https://doi.org/10.1016/0956-7151(95)90165-5.

[26] J.Z. Zhang, A shear band decohesion model for small fatigue carck growth in an ultra-fine grain aluminium alloy, Engineering Fracture Mechanics 65(6) (2000) 665-681, https://doi.org/10.1016/s0013-7944(99)00148-4.

[27] A. Weidner, D. Amberger, F. Pyczak, B. Schönbauer, S. Stanzl-Tschegg, H. Mughrabi, Fatigue damage in copper polycrystals subjected to ultrahigh-cycle fatigue below the PSB threshold, International Journal of Fatigue 32(6) (2010) 872-878, https://doi.org/10.1016/j.ijfatigue.2009.04.004.

[28] S.E. Stanzl-Tschegg, Fracture mechanical characterization of the initiation and growth of interior fatigue cracks, Fatigue and Fracture of Engineering Materials and Structures 40(11) (2017) 1741-1751, https://doi.org/10.1111/ffe.12622.

[29] K. Tanaka, T. Mura, A dislocation model for fatigue crack initiation, Transactions of the ASME, Journal of Applied Mechanics 48(1) (1981) 97-103, https://doi.org/10.1115/1.3157599.

[30] C.A. Sweeney, W. Vorster, S.B. Leen, E. Sakurada, P.E. McHugh, F.P.E. Dunne, The role of elastic anisotropy, length scale and crystallographic slip in fatigue crack nucleation, Journal of the Mechanics and Physics of Solids 61(5) (2013) 1224-1240, https://doi.org/10.1016/j.jmps.2013.01.001.

[31] F. Briffod, T. Shiraiwa, M. Enoki, Modeling and crystal plasticity simulations of lath martensitic steel under fatigue loading, MATERIALS TRANSACTIONS 60(2) (2018) 199-206, https://doi.org/10.2320/matertrans.ME201713.

[32] F. Briffod, T. Shiraiwa, M. Enoki, Microstructure modeling and crystal plasticity simulations for the evaluation of fatigue crack initiation in α-iron specimen including an elliptic defect, Materials Science and Engineering A 695 (2017) 165-177, https://doi.org/10.1016/j.msea.2017.04.030.

[33] D.L. McDowell, F.P.E. Dunne, Microstructure-sensitive computational modeling of fatigue crack formation, International Journal of Fatigue 32(9) (2010) 1521-1542, https://doi.org/10.1016/j.ijfatigue.2010.01.003.

[34] G.M. Castelluccio, D.L. McDowell, Microstructure and mesh sensitivities of mesoscale surrogate driving force measures for transgranular fatigue cracks in polycrystals, Materials Science and Engineering A 639 (2015) 626-639, https://doi.org/10.1016/j.msea.2015.05.048.

[35] K. Tanaka, T. Mura, Fatigue crack growth along planar slip bands, Acta Metallurgica 32(10) (1984) 1731-1740, https://doi.org/10.1016/0001-6160(84)90229-3.

[36] W.H. Peters, W.F. Ranson, M.A. Sutton, T.C. Chu, J. Anderson, Application Of Digital Correlation Methods To Rigid Body Mechanics, Optical Engineering 22(6) (1983) 226738-226738, https://doi.org/10.1117/12.7973231.

[37] J. Carroll, W. Abuzaid, J. Lambros, H. Sehitoglu, An experimental methodology to relate local strain to microstructural texture, Review of Scientific Instruments 81(8) (2010) https://doi.org/10.1063/1.3474902.

[38] C.C. Tasan, J.P.M. Hoefnagels, M.G.D. Geers, Microstructural banding effects clarified through

micrographic digital image correlation, Scripta Materialia 62(11) (2010) 835-838, https://doi.org/10.1016/j.scriptamat.2010.02.014.

[39] C.C. Tasan, J.P.M. Hoefnagels, M. Diehl, D. Yan, F. Roters, D. Raabe, Strain localization and damage in dual phase steels investigated by coupled in-situ deformation experiments and crystal plasticity simulations, International Journal of Plasticity 63 (2014) 198-210, https://doi.org/10.1016/j.ijplas.2014.06.004.

[40] D. Yan, C.C. Tasan, D. Raabe, High resolution in situ mapping of microstrain and microstructure evolution reveals damage resistance criteria in dual phase steels, Acta Materialia 96 (2015) 399-409, https://doi.org/10.1016/j.actamat.2015.05.038.

[41] M. Koyama, T. Ogawa, D. Yan, Y. Matsumoto, C.C. Tasan, K. Takai, K. Tsuzaki, Hydrogen desorption and cracking associated with martensitic transformation in Fe-Cr-Ni-Based austenitic steels with different carbon contents, International Journal of Hydrogen Energy 42(42) (2017) 26423-26435, https://doi.org/10.1016/j.ijhydene.2017.08.209.

[42] R. Kakimoto, M. Koyama, K. Tsuzaki, EBSD and ECCI Based Assessments of Inhomogeneous Plastic Strain Evolution Coupled with Digital Image Correlation, Tetsu-to-Hagane 105(2) (2019) 222-230, https://doi.org/10.2355/tetsutohagane.TETSU-2018-072.

[43] J. Sakamoto, S. Hamada, H. Noguchi, Effects of the shape of small flaws and damage due to a focused ion beam on the fatigue strength characteristics of annealed medium-carbon steel, Engineering Failure Analysis 87 (2018) 49-68, https://doi.org/10.1016/j.engfailanal.2018.02.005.

[44] S. Hamada, T. Fujisawa, M. Koyama, N. Koga, N. Nakada, T. Tsuchiyama, M. Ueda, H. Noguchi, Strain mapping with high spatial resolution across a wide observation range by digital image correlation on plastic replicas, Materials Characterization 98 (2014) 140-146, https://doi.org/10.1016/j.matchar.2014.10.010.

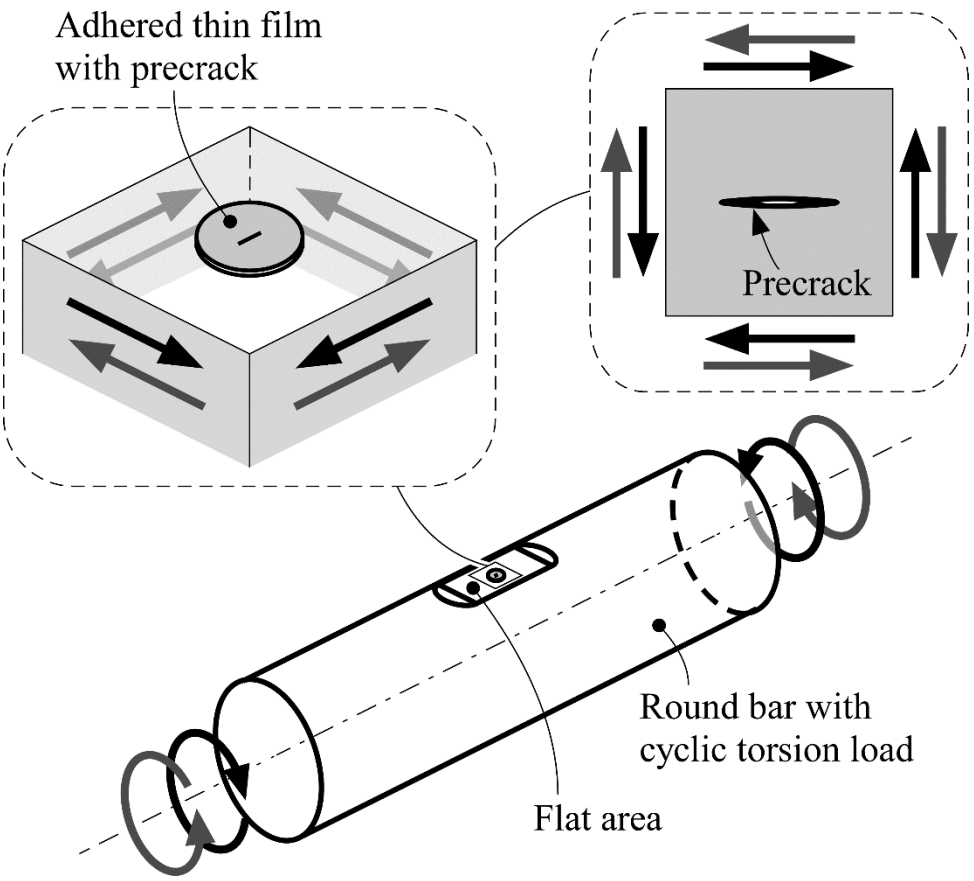

Fig. 1 Schematic of fatigue test [14]

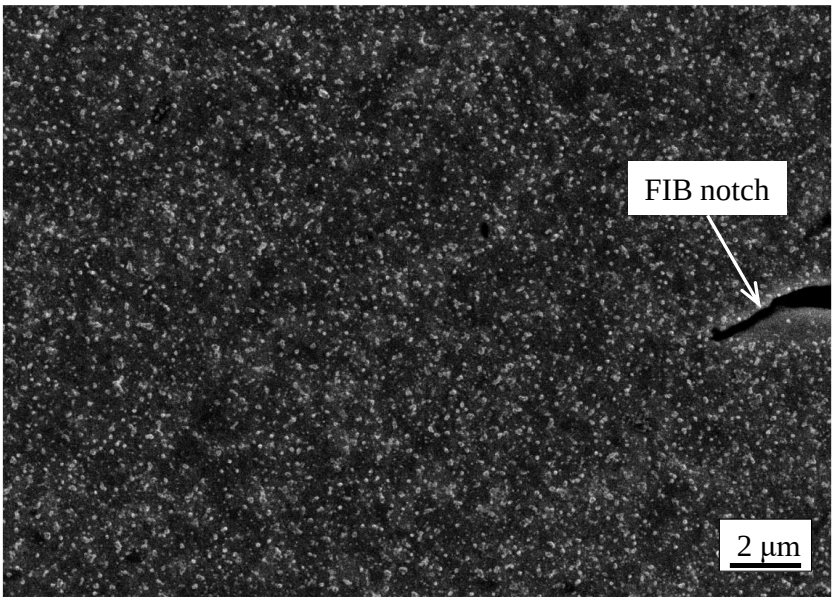

Fig. 2 Around FIB notch chip (N = 0 cycle)

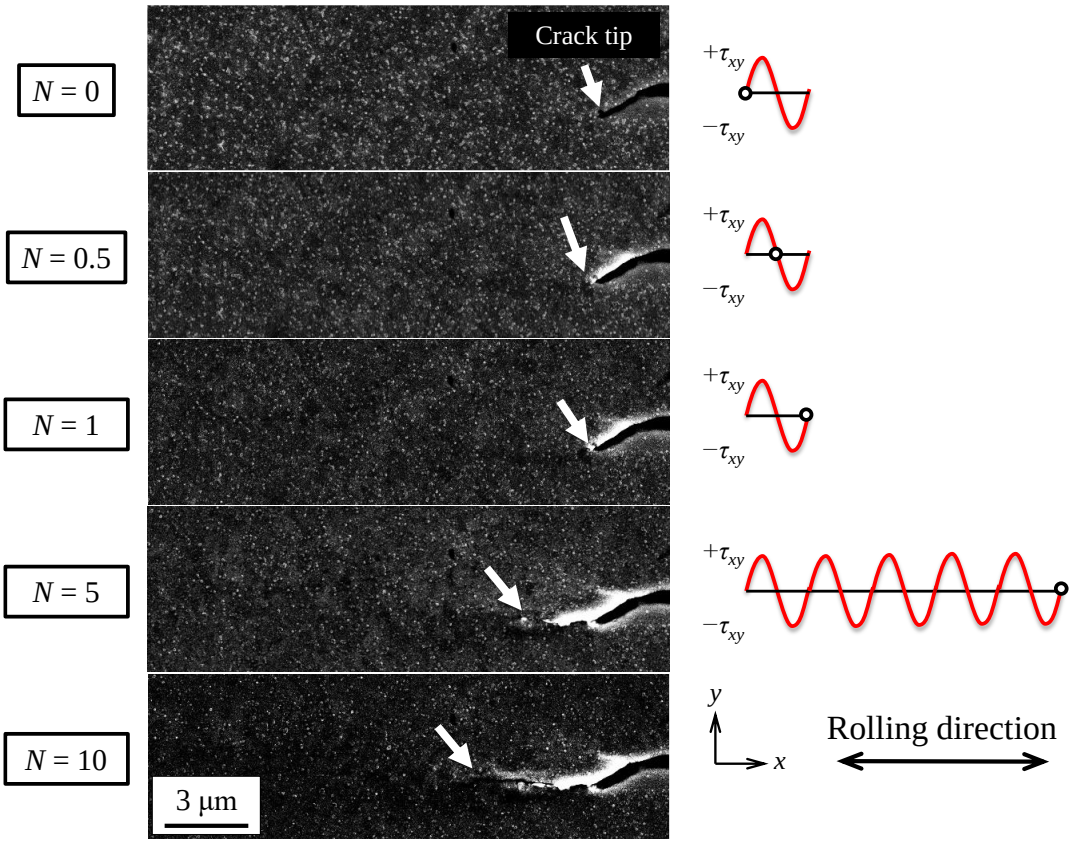

Fig. 3 Fatigue crack propagation behavior during cyclic Mode II loading. τ_a = 200 MPa and R = –1.

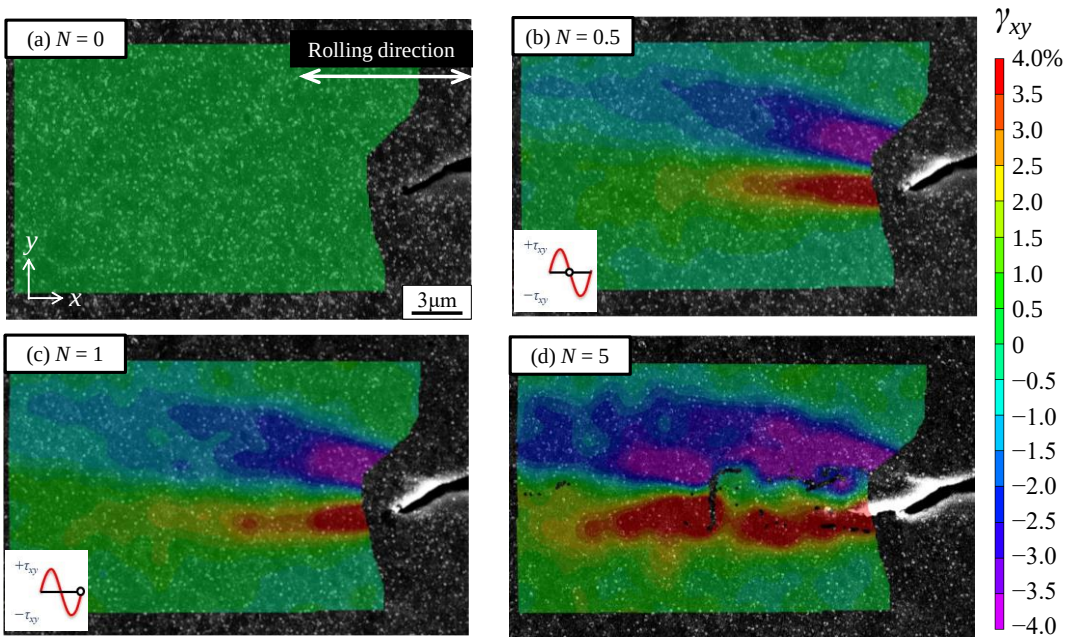

Fig. 4 Shear strain behavior during cyclic Mode II loading. τ_a = 200 MPa and R = –1.

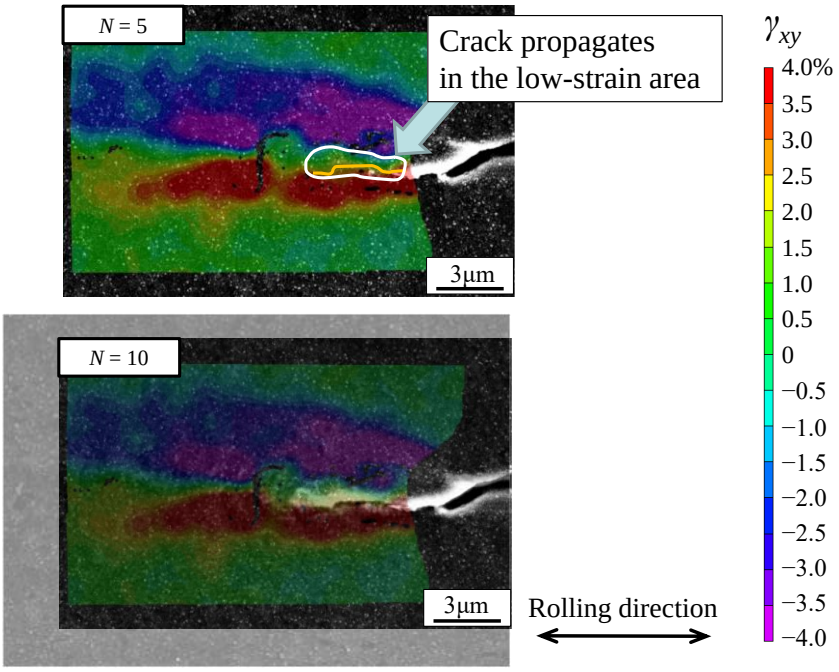

Fig. 5 Relationship between shear strain at the unloading and crack propagation paths.

τ_a = 200 MPa, R = –1.

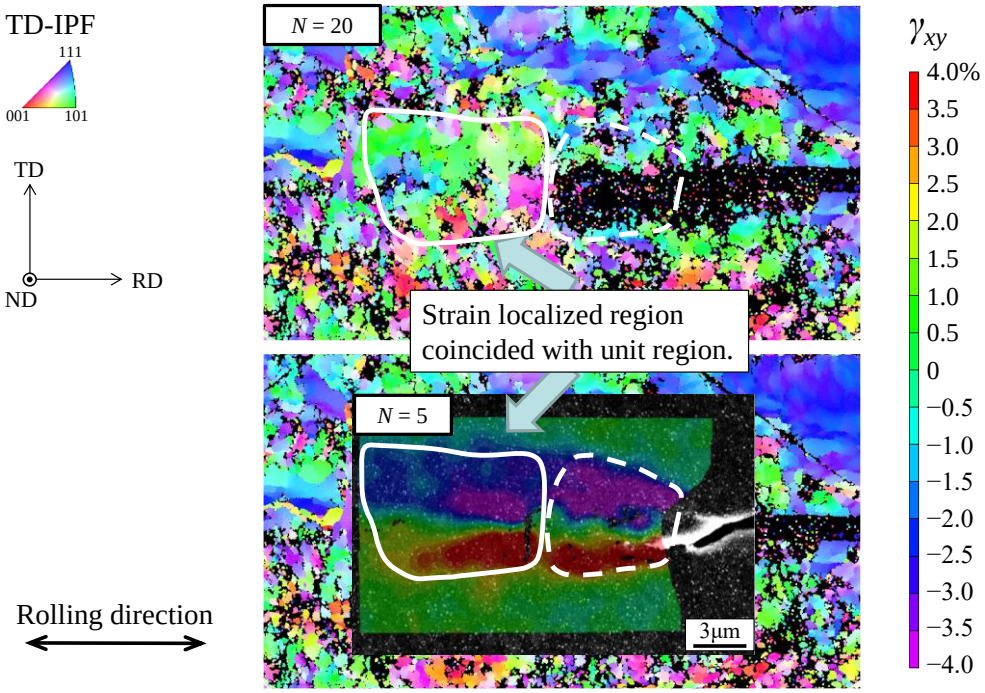

Fig. 6 Relationship between microstructure and shear strain

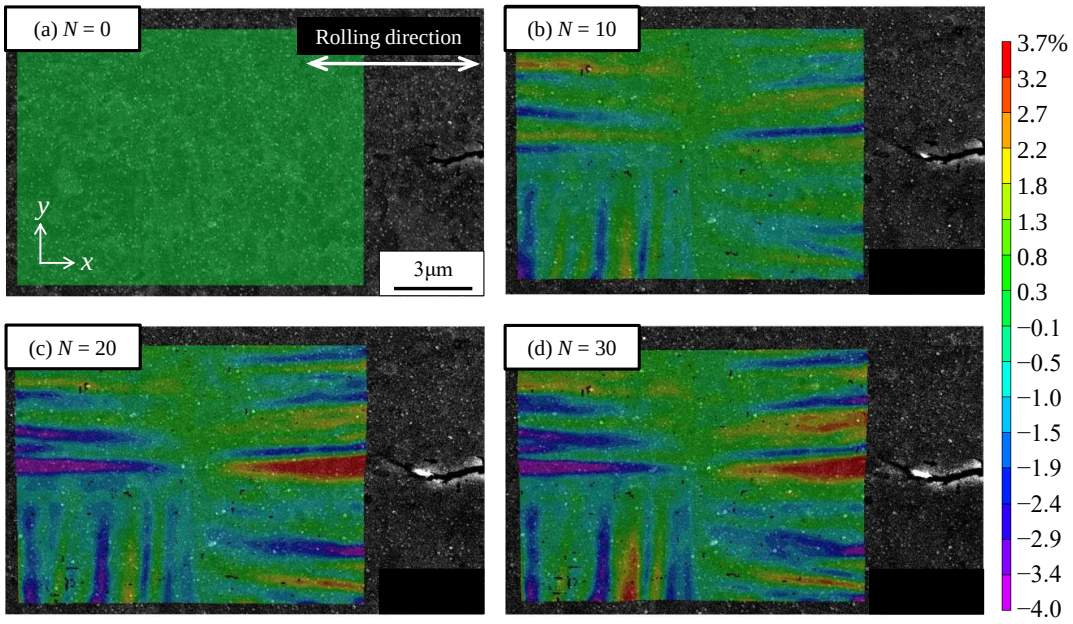

Fig. 7 Shear strain behavior obtained by improper reference length during cyclic Mode II loading

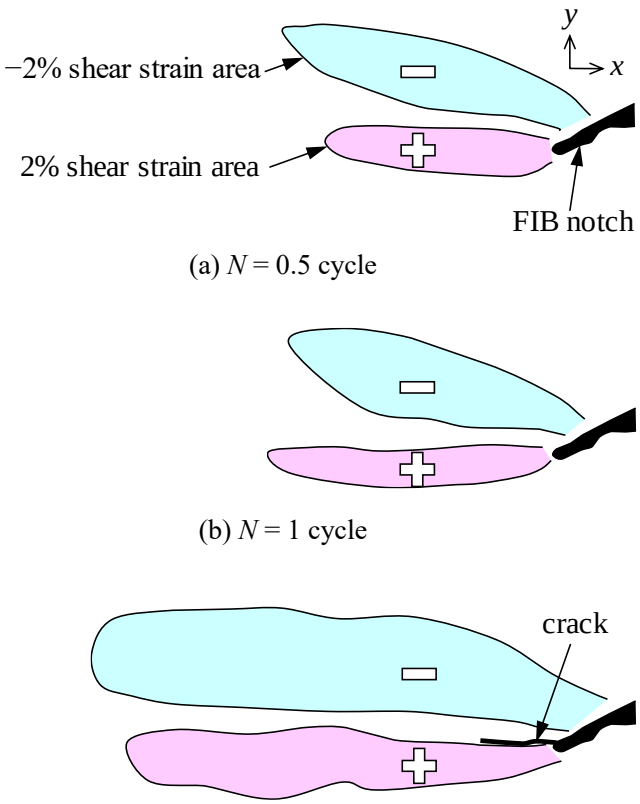

Fig. 8 Schematic of residual shear strain evolution by loading cycles.

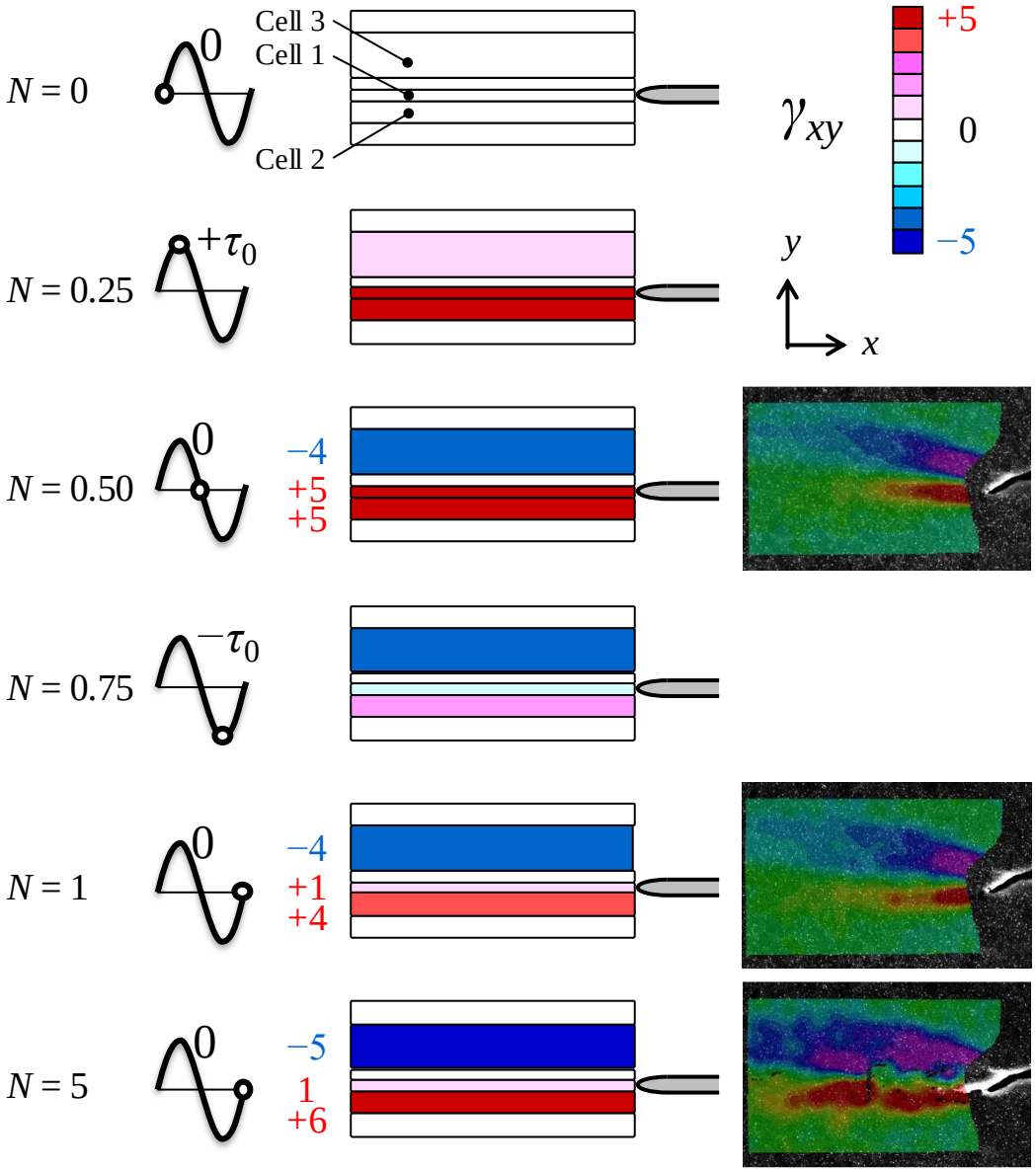

Fig. 9 Introduction of small cell in Fig. 8 and shear strain γ_{xy} on each cell during cyclic loading.

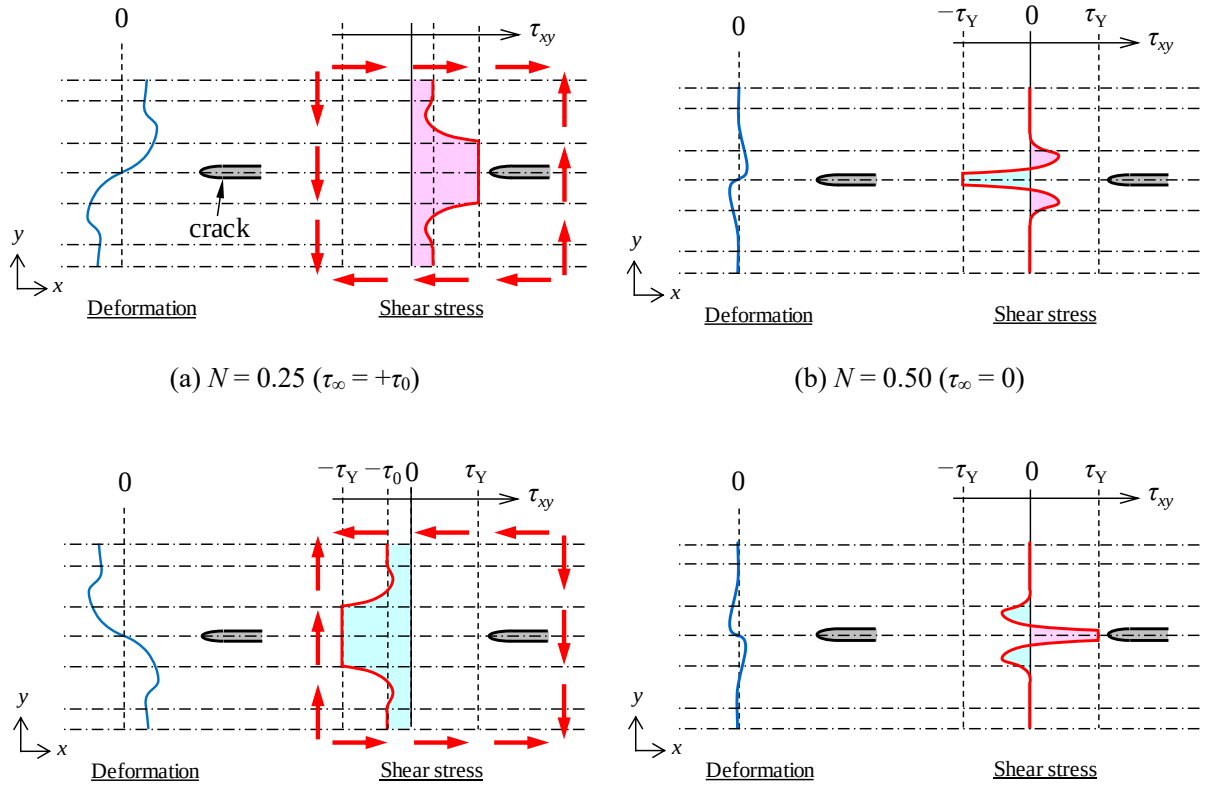

(a) $N = 0.25$ ($\tau_\infty = +\tau_0$)

(b) $N = 0.50$ ($\tau_\infty = 0$)

(c) $N = 0.75$ ($\tau_\infty = -\tau_0$)

(d) $N = 1.0$ ($\tau_\infty = 0$)

Fig. 10 Estimated shear stress τ_{xy} distribution on constant x line ahead of crack tip during cyclic loading.

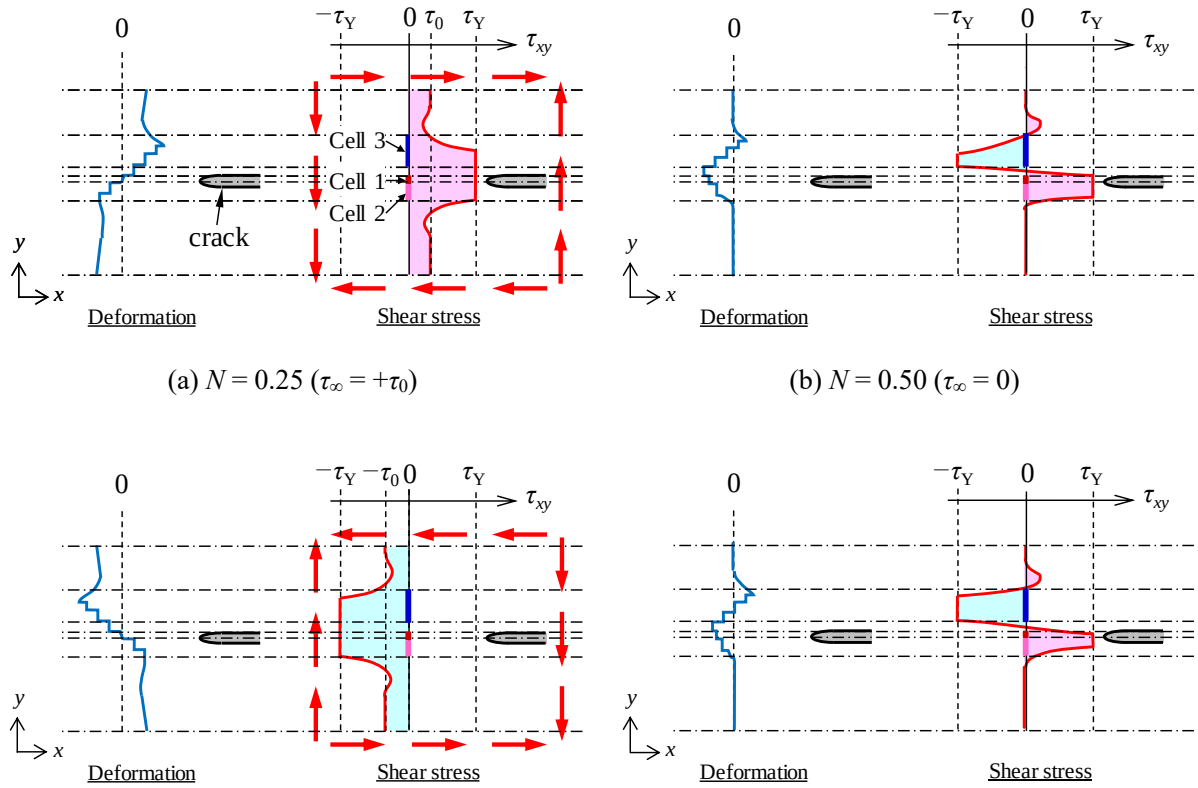

Fig. 11 Estimated shear stress τ_{xy} distribution on constant x line ahead of crack tip during cyclic loading considering slips.

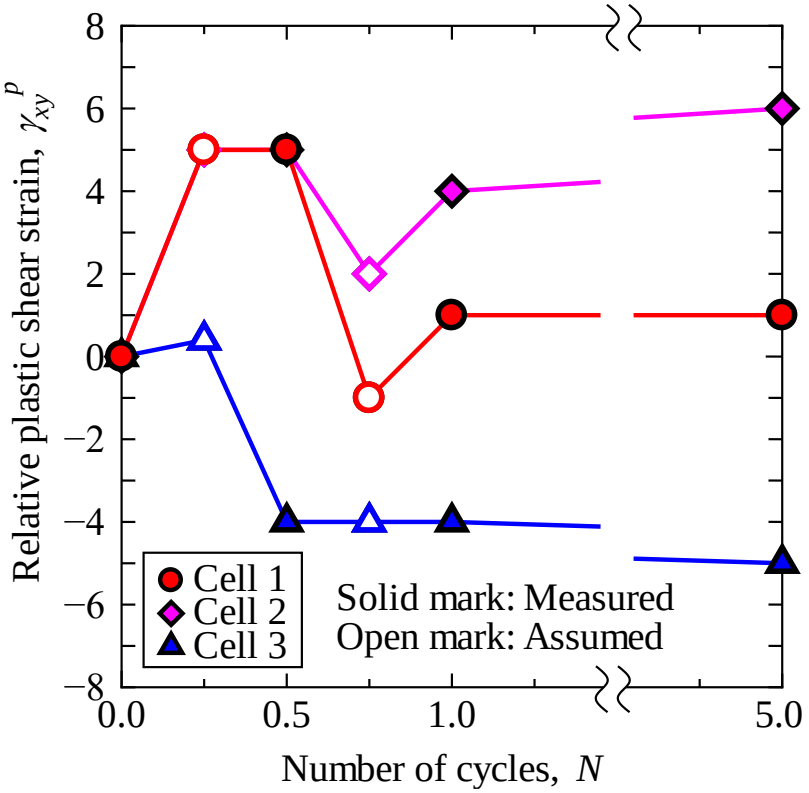

Fig. 12 Estimation of plastic strain changing each small cell.

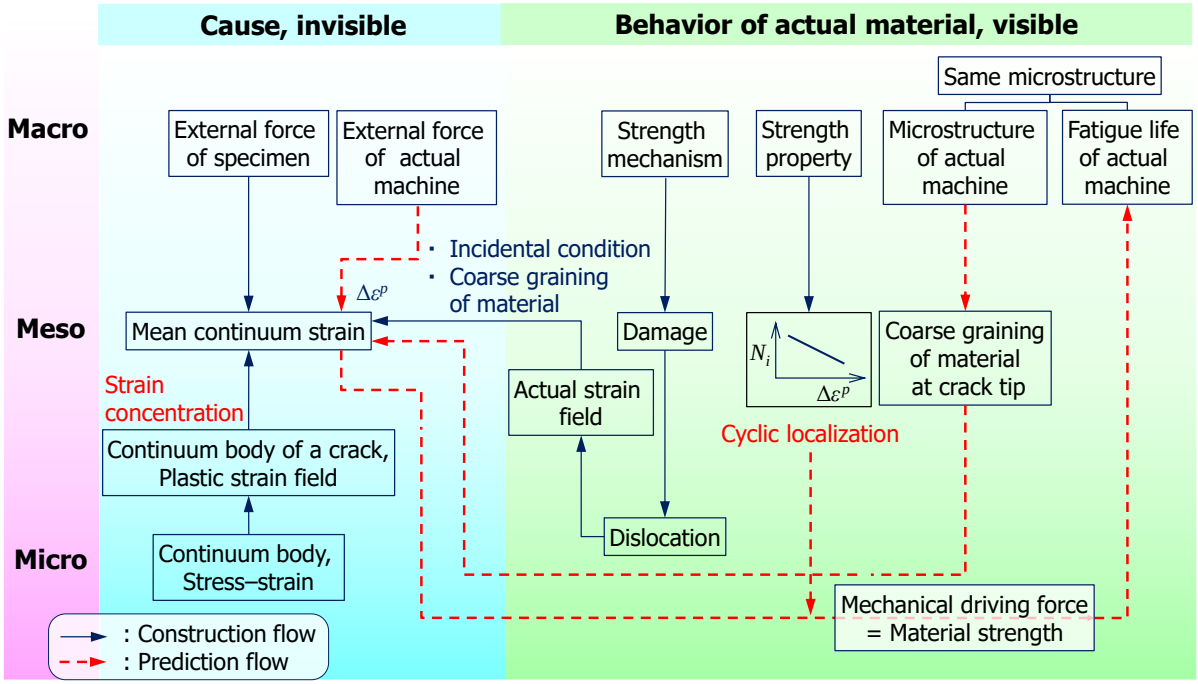

Fig. 13 Damage accumulation mode fatigue crack propagation evaluation strategy

Table 1 Chemical composition of JIS-SUS430 [mass%]

C	Si	Mn	P	S	Cr	Fe
<0.12	<0.75	<1	<0.04	<0.03	16–18	Bal.